

**MINISTÉRIO DA CIÊNCIA E TECNOLOGIA
INSTITUTO NACIONAL DE PESQUISAS ESPACIAIS**

INPE-5523-RPQ/665

**DIGITAL FILTER DESIGN FOR SENSOR SIMULATION:
APPLICATION TO
THE BRAZILIAN REMOTE SENSING SATELLITE**

**Gerald Jean Francis Banon
Ailton Cruz dos Santos**

**INPE
São José dos Campos
Outubro de 1993**

ACKNOWLEDGMENTS

The authors are grateful to Dr. Nelson Delfino d'Ávila Mascarenhas for his help with English usage.

RESUMO

Neste artigo, um modelo de interação, entre um sensor de baixa resolução com largo campo de visada a bordo de um satélite de observação da terra, e a superfície da terra é apresentado. O sensor simulado é obtido através da composição de um algoritmo de simulação digital por um sensor de alta resolução e menor campo de visada. Uma nova técnica de desenvolvimento de filtro digital é proposto para aproximar um filtro Gaussiano ideal. O filtro resultante pode ser implementado em qualquer plataforma existente de processamento de imagens. Finalmente, dois retalhos de imagem, da maneira que eles seriam produzidos pelo SSR (Satelite de Sensoriamento Remoto) da MECB (Missão Espacial Completa Braasileira) a partir de uma cena LANDSAT-TM (Thematic Mapper) são apresentados como exemplo.

ABSTRACT

In this paper, a model of the interaction, between a large-field-of-view low-resolution sensor on board an earth observation satellite, and the earth surface is presented. The simulated sensor is obtained through the composition of a digital simulation algorithm by a smaller field-of-view and higher resolution sensor. A new digital filter design technique is proposed to approximate an ideal Gaussian filter. The resulting filter can be implemented on any existing image processing platform. Finally, two image patches as they would be produced by the SSR (Remote Sensing Satellite) of MECB (Brazilian Complete Spatial Mission) from a LANDSAT-TM (Thematic Mapper) scene are presented as an example.

SUMMARY

	Page
LIST OF FIGURES	xiii
LIST OF TABLE	xv
1 INTRODUCTION	1
2 SENSOR–EARTH SURFACE INTERACTION MODEL	2
2.1 – Set of earth scenes	2
2.2 – Set of digital images	3
2.3 – Sensor model	3
2.4 – Parameters of the sensor model	9
2.5 – IFOVs determination	13
3 SIMULATION PROCESS	15
3.1 – Variances property in linear mappings composition	15
3.2 – Continuous simulation process	19
3.3 – Digital simulation process	19
4 DIGITAL FILTER DESIGN	24
5 APPLICATION TO THE BRAZILIAN REMOTE SENSING SATELLITE	35
5.1 – SSR specifications	36
5.2 – SSR patches specifications	36
5.3 – TM resolution specifications	37
5.4 – Simulation filter specifications and performances	38
6 CONCLUSION	42
REFERENCES	45

LIST OF FIGURES

	Page
1. Graphical illustration of a particular earth scene f	3
2. Graphical illustration of a digital image g	4
3. Sensor model.	5
4. Graphical illustration of a geometrical transformation t	5
5. Graph of the value at u of a particular adaptive point spread function h	6
6. View plane.	7
7. Geometrical construction of $su(x)$ for a point x in the view plane.	8
8. Definition of s and FWHP.	10
9. Definitions of EIFOV and g	11
10. Detector array projection on a tangent plane at nadir.	11
11. Rectangle approximation of a detector projection onto the earth surface (downward view).	13
12. Acquisition geometry of a pixel.	14
13. Alternative option to obtain the blurred earth scene relative to Sensor2.	16
14. Continuous simulation process for Sensor2.	19
15. Digital simulation process for Sensor2.	20
16. Geometrical data involved in the digital simulation algorithm.	22
17. Graph of h_y restricted to M (the grid nodes).	23
18. Graph of f	29
19. Sensor1, Sensor2 and simulated Sensor2 MTF.	35
20. Patch localization in the scene (hatch area).	37
21. MTFs' comparison.	39
22. Buritama reservoir and Araçatuba, Birigui e Penápolis cities (São Paulo State). SSR Band 1 patch obtained by SSR simulation from TM5 Band 3, orbit 222, point 75, quadrant B, June 27, 1987.	41
23. Buritama reservoir and Araçatuba, Birigui e Penápolis cities (São Paulo State). SSR Band 2 patch obtained by SSR simulation from TM5 Band 4, orbit 222, point 75, quadrant B, June 27, 1987.	42

LIST OF TABLES

	Page
1 – Resolution parameters relationships in the Gaussian case.	12
2 – Filter design parameters.	31
3 – SSR specifications.	36
4 – SSR patches specifications.	36
5 – TM resolution specifications.	37

1 INTRODUCTION

In order to evaluate the future images that would be produced by the SSR (Remote Sensing Satellite) of MECB (Brazilian Complete Spatial Mission), an important task is to perform some previous sensor simulations.

The simulated large-field-of-view low-resolution sensor is obtained through the composition of a digital simulation algorithm with a smaller field-of-view and higher resolution sensor. The digital simulation algorithm consists in a batteries of linear digital filters.

In this paper, we propose a new technique to design such linear digital filters. This technique is based on the assumption that the MTF (Modulation Transfer Function) of both sensors can be approximated by a centered Gaussian type function (Leger et al., 1986). With this assumption, the 2D MTF of the ideal simulation filter is Gaussian and simply characterized by two parameters. With these two parameters at hands, the proposed design technique consists in specifying the parameters of the simulation digital filter. The digital filter is supposed to be the convolution product extended to n identical Moving Average (MA) filters whose coefficients follow a Gaussian law. The parameters to be specified are the size N of the impulse response support of the MA filters and the number $n - 1$ of convolution products. These parameters must satisfy an inequality relation that derives from the spread constraints on the impulse response of the digital filter to be designed. Once the parameters N and n are chosen, the coefficients of the MA filters are obtained by solving a polynomial equation.

In Section 2, we present the sensor-earth surface interaction model. The definition of some usual resolution parameters and their relationships are recalled. Because the simulated sensor has a wide field-of-view, the earth surface curvature has to be considered and the resolution parameter value changes from point to point.

In Section 3, we introduce the simulation process. This process consists in applying linear digital filters to the images produced by a high resolution sensor and to derive the pixel values of the simulated image by interpolation. Such filters are typically non translation invariant and have adaptive finite impulse response.

In Section 4, we introduce the digital filter design technique.

Finally, in Section 5, we use and evaluate the above technique through the simulation of the sensor on board the SSR. For such sensor simulation, the design filters are applied to LANDSAT-TM (Thematic Mapper) images.

2 SENSOR-EARTH SURFACE INTERACTION MODEL

The sensor on board an earth observation satellite transforms any earth scene into a collection of digital images. We will denote an earth scene by f and a digital image by g .

2.1 – SET OF EARTH SCENES

By a *earth scene* f , we actually mean an equivalent scene with respect to a given spectral sensitive curve (Begni et al., 1986), that is, assuming that the scene is Lambertian, f can be seen simply as a function from a surface S (representing the earth surface) to \mathbb{R} , the set of real numbers (a subset of which representing all the possible spectral radiance values with respect to a given spectral sensitivity curve – one for each spectral band of the sensor). Mathematically, we write $f \in \mathbb{R}^S$. Figure 1 shows a graphical illustration of a particular earth scene f . With respect to the point x on the earth surface S , the earth scene f assumes the spectral radiance value $f(x)$.

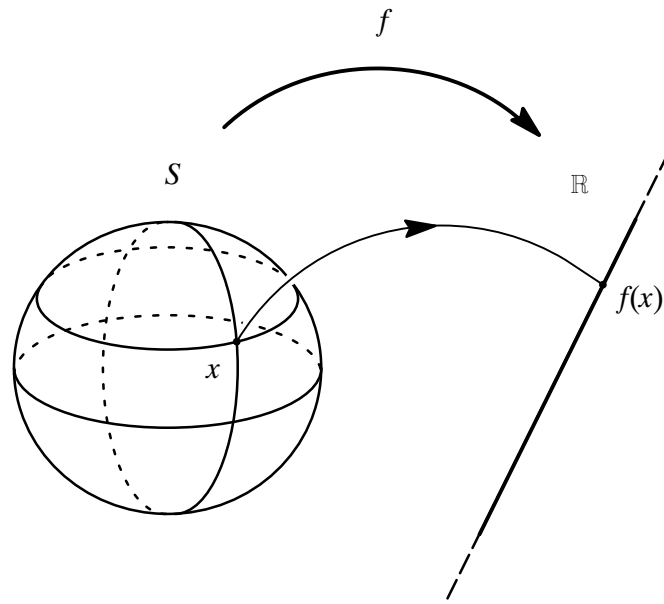


Fig. 1. Graphical illustration of a particular earth scene f .

2.2 – SET OF DIGITAL IMAGES

A *digital image* g is a function from a subset E of \mathbb{R}^2 , the set of real pairs, to \mathbb{R} . A pair $(y, g(y))$ formed by an element y of E and the corresponding element $g(y)$ of \mathbb{R} through g is called *pixel of g* . Given the pixel $(y, g(y))$, y is called its *position* and $g(y)$ its *value*. Mathematically, we write $g \in \mathbb{R}^E$. Figure 2 shows a graphical illustration of a particular digital image g that has as domain E a rectangle of \mathbb{Z}^2 , the set of integer pairs. With respect to the position y in E , the digital image g assumes the value $g(y)$.

In Figure 2, the array of black points represents the set E of pixel positions.

2.3 – SENSOR MODEL

By sensor model we mean a model for the sensor–earth surface interaction. The model for the sensor is represented as a collection of functions ψ_i , $i = 1, \dots, m$, where the i^{th} function ψ_i transforms an earth scene f into an i^{th} digital image g_i .

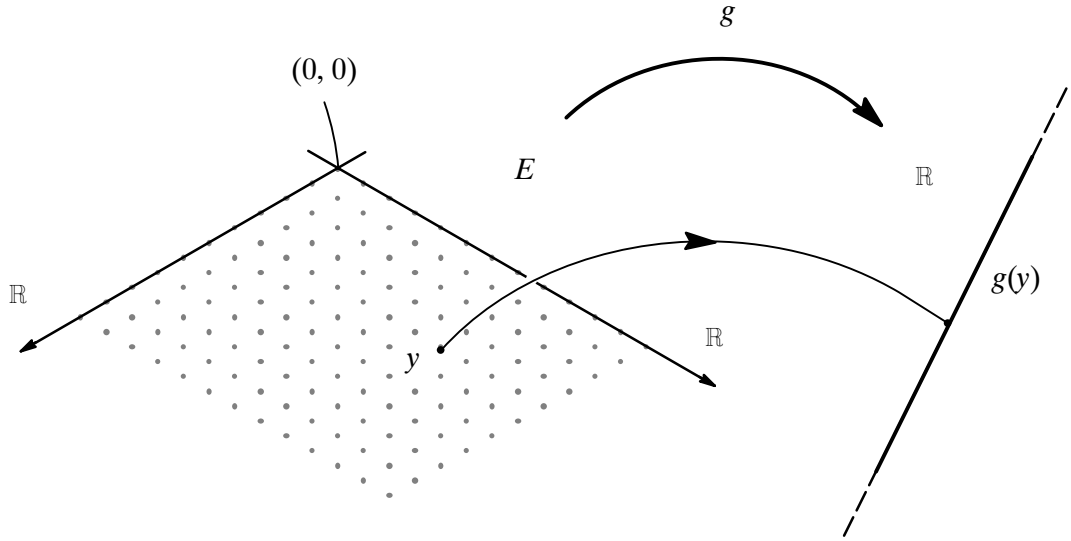


Fig. 2. Graphical illustration of a digital image g .

For passive sensors, like the “Thematic Mapper” (TM–LANDSAT), the “Haute Résolution Visible” (HRV–SPOT) and the “Satélite de Sensoriamento Remoto” (SSR–MECB), if we disregard the digital conversion process, we can assume that each ψ_i is the composition of a Sampling Process (SP) represented by a geometrical transformations t_i from \mathbb{R}^2 to S with a Continuous Linear Mapping (CLM) represented by a function h_i from S to \mathbb{R}^S , that is, for any earth scene $f \in \mathbb{R}^S$ and any pixel position $y \in E$,

$$g_i(y) = (\psi_i(f))(y) = \int_S f(u)h_i(u)(t_i(y))du, \quad i = 1, \dots, m. \quad (1)$$

We will denote a collection of m digital images produced by the sensor by $\{g_i\}_1^m$ or simply $\{g_i\}$. Figure 3 gives a graphical illustration of the sensor model.

A particular geometrical transformation t_i , or simply t , maps any pixel position y in $E (\subset \mathbb{R}^2)$ to the point $t(y)$ on the earth surface S (see Figure 4). At each pixel position y , it corresponds a given detector and a given instant. The point $t(y)$ is the projection on the earth surface, through the sensor, of the center of such detector at that instant.

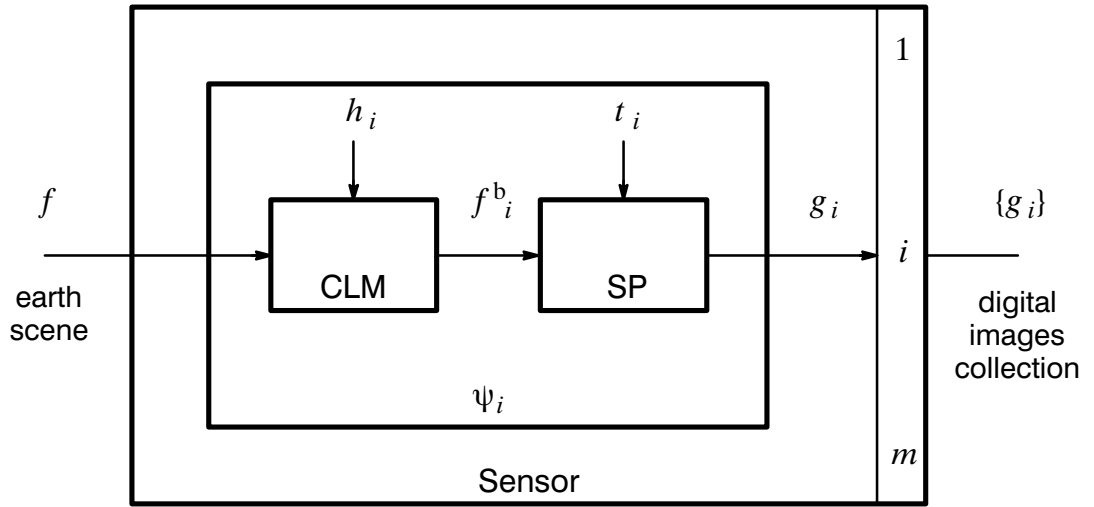
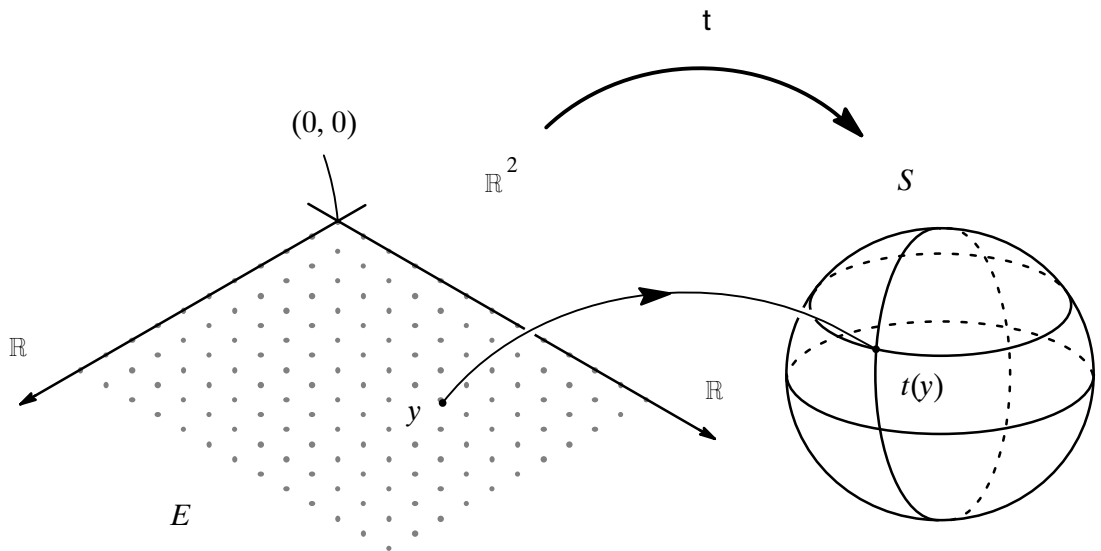


Fig. 3. Sensor model.

Fig. 4. Graphical illustration of a geometrical transformation t .

A particular continuous linear mapping from \mathbb{R}^S to \mathbb{R}^S , represented by h_i , or simply h , transforms an earth scene f into a *blurred earth scene* f^b . In other words, for any earth scene $f \in \mathbb{R}^S$ and for any $x \in S$,

$$f^b(x) = \int_S f(u)h(u)(x)du. \quad (2)$$

The blurred earth scene indicates how the sensor “see” the original earth scene.

The value at u in S of h is a function that maps any point x in S to the real value $h(u)(x)$ (see Figure 5). The function h is called *adaptive point spread function of*

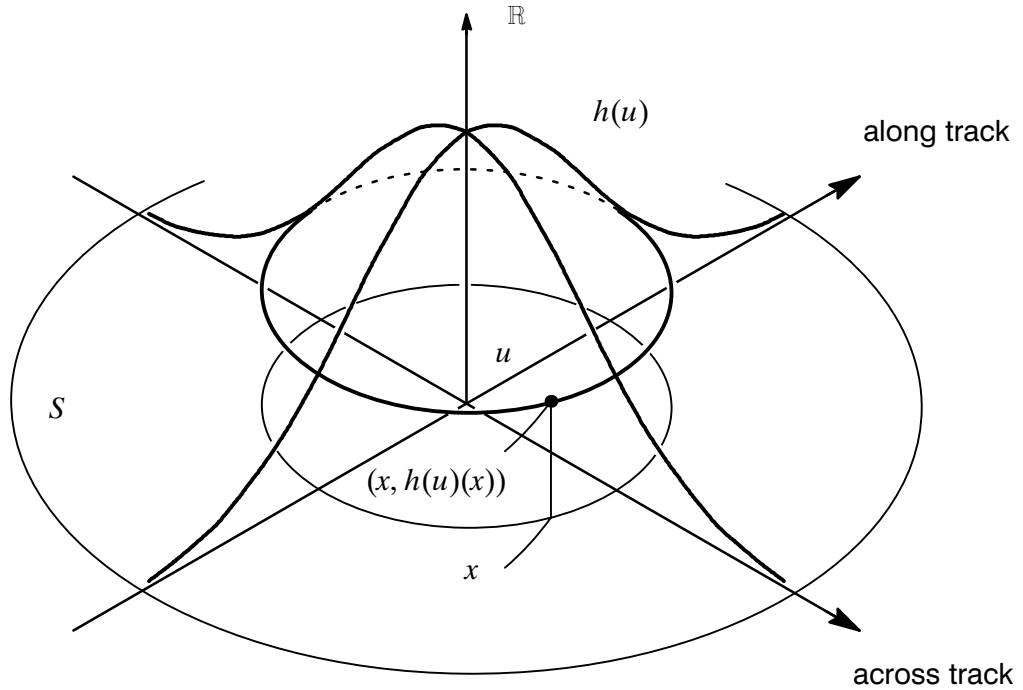


Fig. 5. Graph of the value at u of a particular adaptive point spread function h .

the sensor. The adaptive point spread function defines the *spatial resolution of the sensor* at the earth surface level.

A particular function $h(u)$ can be interpreted as the transformation of an ideal point scene δ_u , the Dirac function from S to \mathbb{R} located at u , by the continuous linear mapping given by Expression (2), that is, for any $x \in S$,

$$h(u)(x) = \int_S \delta_u(v)h(v)(x)dv. \quad (3)$$

The above sensor model is appropriate for large-field-of-view sensors. Because of the sphericity of the earth, the sensor-earth surface interaction model is not

translation invariant. In other words, the transformation of an ideal point scene is position dependent and the point spread functions have to be adaptive.

Finally, from Expressions (1) and (2), we observe that at position y the pixel value $g(y)$ produced by the sensor is simply a sample of the blurred earth scene located at $t(y)$,

$$g(y) = f^b(t(y)). \quad (4)$$

We call *detectors line* the smaller straight line segment that contains all the detector centers and *view plane* the plane that contains the optical center p of the telescope and the virtual detectors line (see Figure 6.)

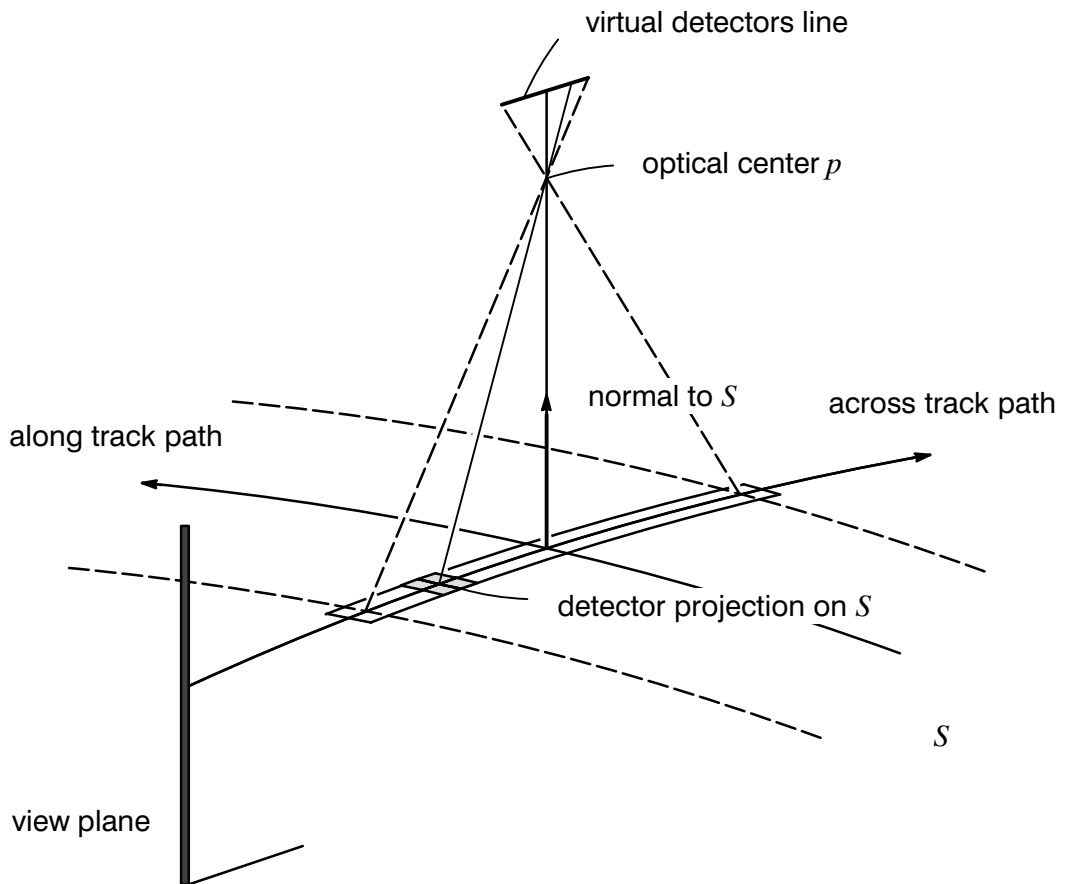


Fig. 6. View plane.

In order to get a tractable model for the sensor–earth surface interaction, the earth surface will be assumed *ellipsoidal*, the view plane will contain a normal at S that passes through the optical center of the telescope, and the value at u of the adaptive point spread function of the sensor will be derived from a *separable* real valued function $h'(u)$ defined on T_u , the tangent plane in u at S , that is, for any $x \in S$,

$$h(u)(x) = \begin{cases} h'(u)(s_u(x)) & \text{if } x \in S_p, \\ 0 & \text{otherwise,} \end{cases} \quad (5)$$

where p is the optical center of the telescope in the view plane that contains u (see Figure 7);

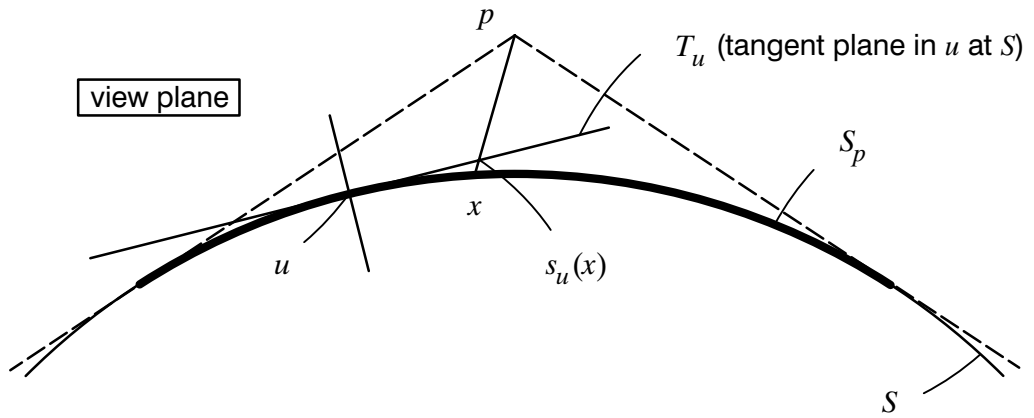


Fig. 7. Geometrical construction of $s_u(x)$ for a point x in the view plane.

where S_p is the set of points x of S that are “visible” from the optical center p (see Figure 7);

where $s_u(x)$ is the intersection between the straight line xp and the tangent plane T_u (see Figure 7).

Because of the drastically different scales between the ellipsoidal earth surface and the spatial resolution of the sensor, we can approximate the earth surface S around the point u by its tangent plane T_u . For that reason, we will also call h' the adaptive point spread of the sensor and will denote it simply by h .

The above *separability assumption* on h means that there exists two functions $h_1(u)$ and $h_2(u)$ from \mathbb{R} to \mathbb{R} such that, for any u in S and z in T_u ,

$$h(u)(z) = h_1(u)(z_1)h_2(u)(z_2), \quad (6)$$

where z_1 and z_2 are the coordinates of the point z with respect to the coordinate system with origin in u and formed by the tangents in u at the along track and across track paths drawn on S , respectively.

The functions h_1 and h_2 are called *1-D adaptive point spread functions for the along track and across track directions*, respectively, and they define the spatial resolution of the sensor for these two directions.

2.4 – PARAMETERS OF THE SENSOR MODEL

In this subsection, we recall the definitions of some usual resolution parameters and their relationships.

Let us denote simply by h the value at $u \in S$ of any of both 1-D adaptive point spread functions. We will use the letter H to represent the Fourier Transform of h . For a symmetrical function h such that $H(0) = 1$, the value at u of the *1-D adaptive modulation transfer function* of the sensor for the chosen direction $|H/H(0)|$ is simply H . For the sake of simplicity, we will refer to h as a *point spread function* and to H as a *Modulation Transfer Function* (MTF).

The *variance* (using the Probability Theory terminology) of the function h , denoted by σ^2 , is the positive real number given by

$$\sigma^2 = \left(\int_{\mathbb{R}} (x - \mu)^2 h(x) dx \right) / \left(\int_{\mathbb{R}} h(x) dx \right), \quad (7)$$

where

$$\mu = \left(\int_{\mathbb{R}} xh(x)dx \right) / \left(\int_{\mathbb{R}} h(x)dx \right). \quad (8)$$

Figure 8 shows the *standard deviation* σ for a given symmetrical function h .

The *Full Width Half Peak* of the function h , denoted FWHP, is the positive real number that satisfies (see Figure 8)

$$\left(\frac{\text{FWHP}}{2}, \frac{h(0)}{2} \right) \in \text{graph of } h. \quad (9)$$

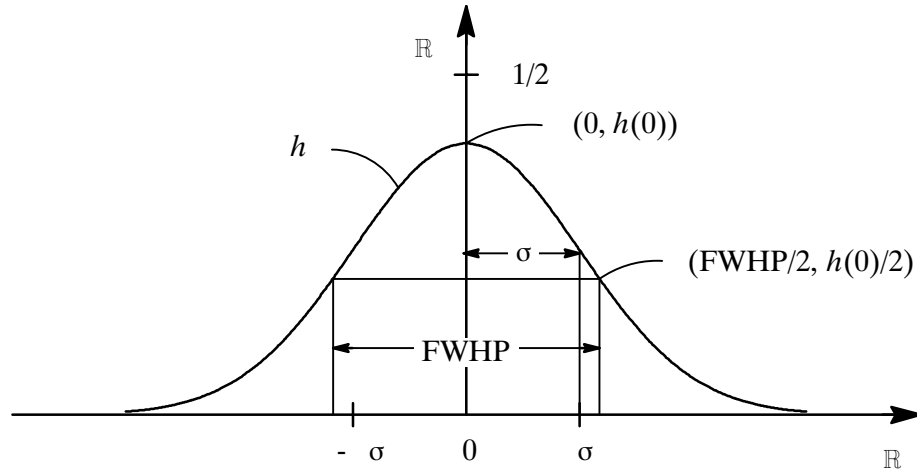


Fig. 8. Definition of σ and FWHP.

The *Effective Instantaneous Field Of View* of the function h , denoted EIFOV, is the positive real number that satisfies (see Figure 9)

$$\left(\frac{1}{2\text{EIFOV}}, \frac{1}{2} \right) \in \text{graph of } H/H(0). \quad (10)$$

The *attenuation factor* of the modulation transfer function at half the sampling frequency ν for the chosen direction, denoted γ , is the real number that satisfies (see Figure 9)

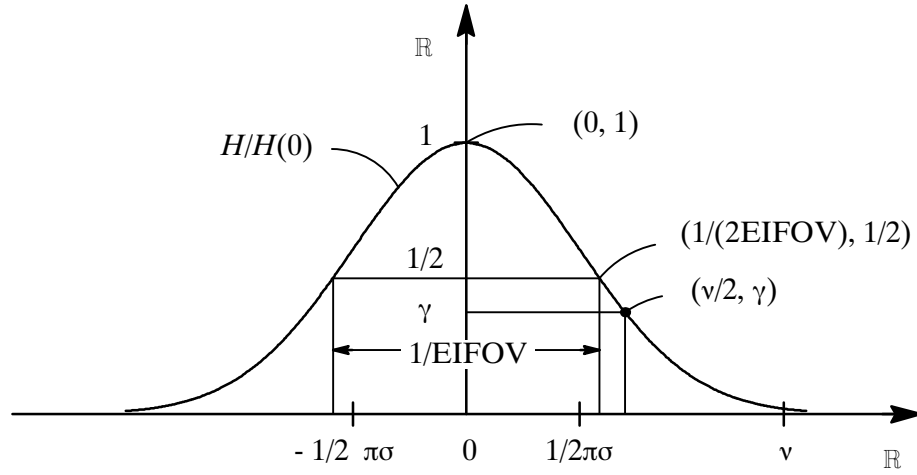


Fig. 9. Definitions of EIFOV and γ .

$$\left(\frac{v}{2}, \gamma\right) \in \text{graph of } H/H(0). \quad (11)$$

The sampling frequency v for the chosen direction is $1/\delta$, where δ is the *distance between two consecutive sample positions* along that direction (see Figure 10.)

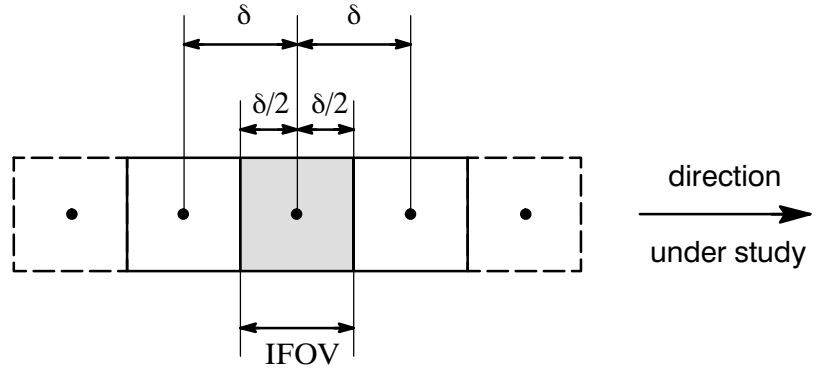


Fig. 10. Detector array projection on a tangent plane at nadir.

If we assume that h is a 1-D Gaussian function with variance σ^2 , that is,

$$h(x) = \frac{1}{\sigma(2\pi)^{1/2}} \exp\left(-\frac{x^2}{2\sigma^2}\right) \quad (x \in \mathbb{R}), \quad (12)$$

then the function H is given by

$$H(y) = \exp(-2\pi^2\sigma^2 y^2) \quad (y \in \mathbb{R}), \quad (13)$$

and we can establish, from Expressions (9)–(13), the following relationships between the parameters σ , FWHP, EIFOV and δ (Banon,1990)

$$\frac{\text{FWHP}}{\sigma} = (8\ln(2))^{1/2} (= 2.35482), \quad (14)$$

$$\frac{\text{EIFOV}}{\sigma} = \pi(2\ln(2))^{-1/2} (= 2.66822), \quad (15)$$

$$\frac{\delta}{\sigma} = \pi(2\ln(1/\gamma))^{-1/2} (= 2.16809 \text{ for } \gamma = 0.35). \quad (16)$$

Expression (16) can still be written

$$\gamma = \exp\left(-\frac{\pi^2\sigma^2}{2\delta^2}\right). \quad (17)$$

Table 1 gives the numerical relationships between the above parameters for $\gamma = 0.35$.

TABLE 1 – RESOLUTION PARAMETERS RELATIONSHIPS IN THE GAUSSIAN CASE.

	σ	FWHP	EIFOV	$\delta (\gamma = 0.35)$
$\sigma =$	-	$0.42466 \times \text{FWHP}$	$0.37478 \times \text{EIFOV}$	$0.46124 \times \delta$
FWHP =	$2.35482 \times \sigma$	-	$0.88254 \times \text{EIFOV}$	$1.08613 \times \delta$
EIFOV =	$2.66822 \times \sigma$	$1.13309 \times \text{FWHP}$	-	$1.23068 \times \delta$
$\delta (\gamma = 0.35) =$	$2.16809 \times \sigma$	$0.92070 \times \text{FWHP}$	$0.81256 \times \text{EIFOV}$	-

If, for the chosen direction, the distance δ between two consecutive sample positions is equal to the *instantaneous field of view*, denoted IFOV, as shown in Figure 10, then we can establish from Expression (16) the following relationships between σ and IFOV

$$\sigma = \frac{1}{\pi}(2\ln(1/\gamma))^{1/2} \text{IFOV}. \quad (18)$$

In particular, for $\gamma = 0.35$, from Table 1,

$$\sigma = 0.46124 \times \text{IFOV}. \quad (19)$$

$$\text{FWHP} = 1.08613 \times \text{IFOV}. \quad (20)$$

$$\text{EIFOV} = 1.23068 \times \text{IFOV}. \quad (21)$$

For both directions, the parameters γ , σ , FWHP and EIFOV depend on the point u on the earth surface, and they define, in the neighborhood of u , the spatial resolution of the sensor. The greater is γ or the smaller are σ , FWHP and EIFOV, and the thinner is the spatial resolution.

2.5 – IFOVS DETERMINATION

For a given $u \in S$, we are interested in finding the size IFOV_1 and IFOV_2 of a rectangle in the tangent plane in u at S which projection on S best approximates the detector projection on the earth surface (see Figure 11.) For this purpose, we will con-

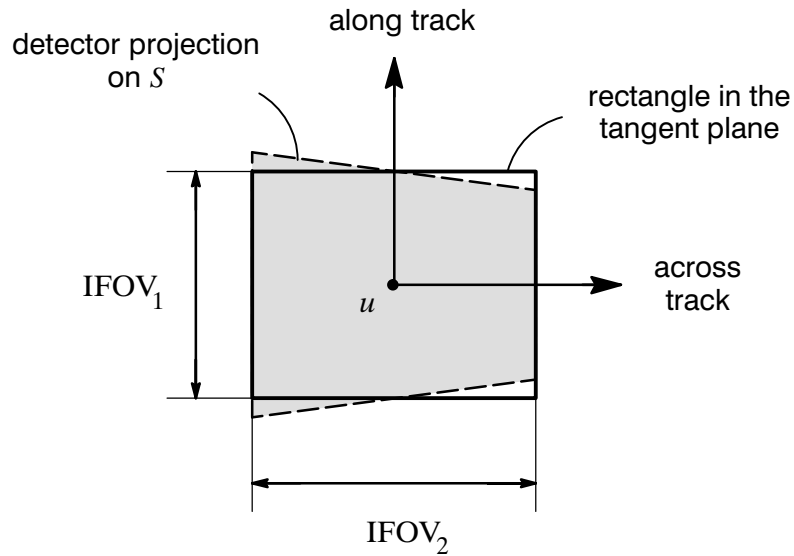


Fig. 11. Rectangle approximation of a detector projection onto the earth surface (downward view).

sider the curvature of the S section in the view plane that contains u .

We now consider the following parameters within the view plane (see Figure 12):

let q be the orthogonal projection of the optical center p onto the earth surface;

let r be the length of the segment up ;

let d be the size of the square representing the detector shape;

let f be the focal length of the telescope;

let θ be the view angle upq ;

let c be the curvature center;

let θ_c be the angle ucq ;

let r_c be the curvature radius at u ;

let h be the satellite altitude.

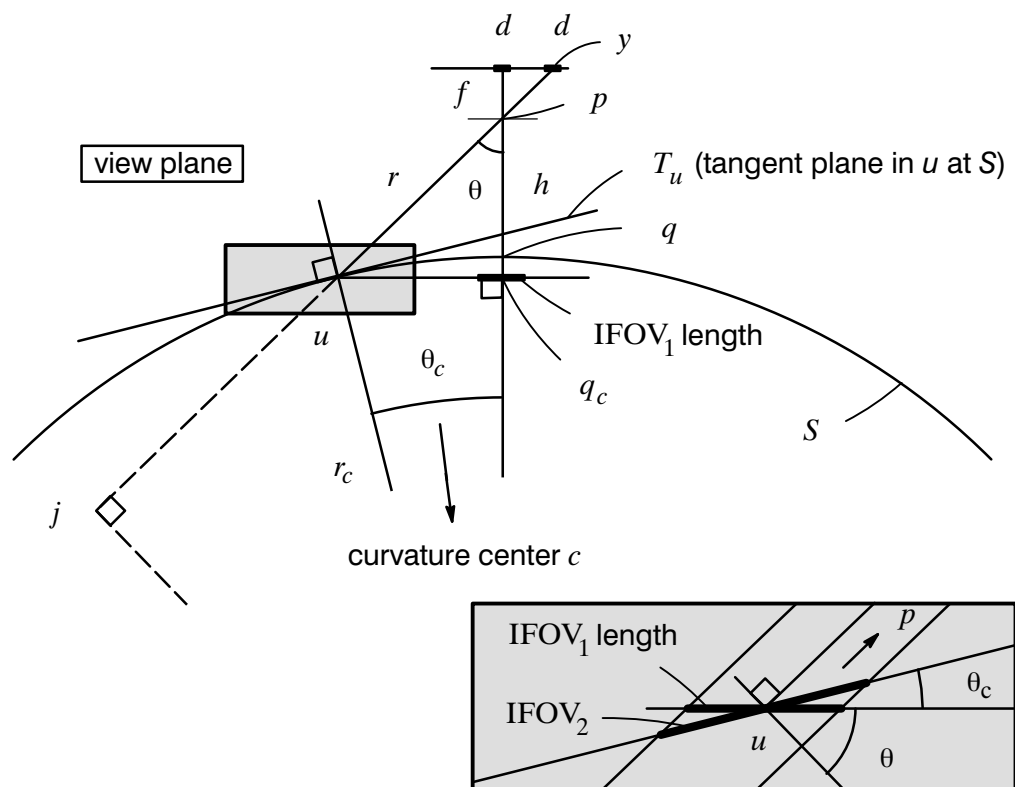


Fig. 12. Acquisition geometry of a pixel.

From Figure 12 we can establish that

$$\text{IFOV}_1 = r \cos(|\theta|) (d/f) \quad (\text{from triangle } uq_c p), \quad (22)$$

$$\text{IFOV}_2 = \text{IFOV}_1 \cos(|\theta|) / \cos(|\theta| + \theta_c) \quad (\text{from the zoomed part of Figure 12}), \quad (23)$$

$$r = (r_c + h) \cos(|\theta|) - (r_c^2 - (r_c + h)^2 \sin^2(|\theta|))^{1/2} \quad (\text{from triangles } jpc \text{ e } juc), \quad (24)$$

$$\theta_c = \arcsen(r \sin(|\theta|) / r_c) \quad (\text{from triangles } uq_c p \text{ e } uq_c c). \quad (25)$$

In other words, under the Gaussian assumption and $\gamma = 0.35$, for a given $u \in S$, the parameters $\sigma_1(u)$ and $\sigma_2(u)$, in the expression of $h(u)(z)$,

$$h(u)(z_1, z_2) = \frac{1}{2\pi\sigma_1(u)\sigma_2(u)} \exp\left(-\left(\frac{z_1^2}{2\sigma_1(u)^2} + \frac{z_2^2}{2\sigma_2(u)^2}\right)\right) \quad ((z_1, z_2) \in T_u), \quad (26)$$

are given by, from Expression (19),

$$\sigma_1(u) = 0.46124 \times \text{IFOV}_1, \quad (27)$$

$$\sigma_2(u) = 0.46124 \times \text{IFOV}_2, \quad (28)$$

where IFOV_1 e IFOV_2 are obtained from Expressions (22) to (25).

3 SIMULATION PROCESS

3.1 – VARIANCES PROPERTY IN LINEAR MAPPINGS COMPOSITION

Let $h1$ and $h2$ be the adaptive point spread function of two sensors called here *Sensor1* and *Sensor2*, respectively. Let us assume that $h1$ and $h2$ are such that, for any $u \in S$, there exists a unique function $\tilde{h}(u)$ from S to \mathbb{R} such that, for any $x \in S$,

$$h2(v)(x) = \int_S h1(v)(u) \tilde{h}(u)(x) du \quad (v \in S). \quad (29)$$

If $f1^b$ and $f2^b$ are the blurred earth scene obtained by transformation of the earth scene f through the continuous linear mappings represented, respectively, by $h1$

and h_2 , then the above assumption guarantees that f_2^b can be derived from f_1^b through the continuous linear mapping represented by \mathcal{H} . More precisely, for any $x \in S$,

$$f_2^b(x) = \int_S f_1^b(u) \mathcal{H}(u)(x) du. \quad (30)$$

This result is illustrated in Figure 13 .

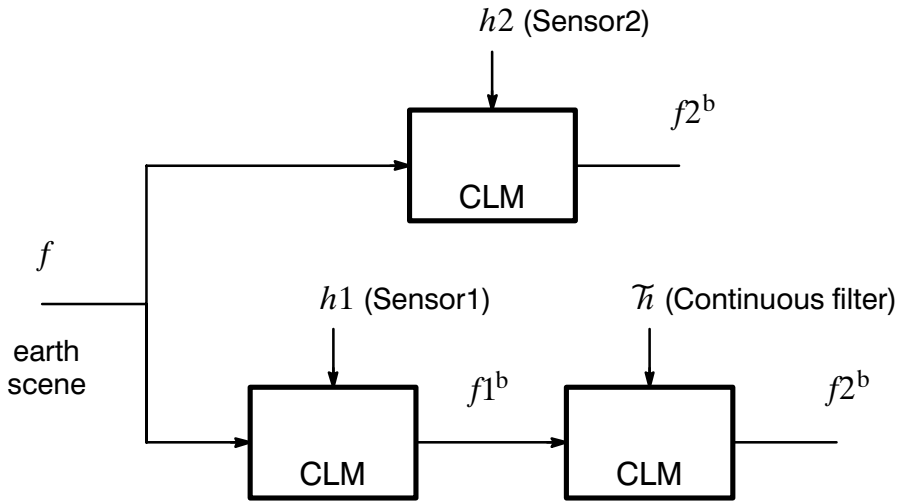


Fig. 13. Alternative option to obtain the blurred earth scene relative to Sensor2.

Let us approximate, as in Subsection 2.3, the earth surface S around the point v in S by its tangent plane T_v and let us assume that there exists a unique function \mathcal{H}_v from T_v to \mathbb{R} such that, for any $z \in T_v$,

$$h_2(v)(z) = \int_{T_v} h_1(v)(u) \mathcal{H}_v(z - u) du. \quad (31)$$

Returning to the separability assumption of Subsection 2.3, Expression (31) also applies to the 1-D adaptive point spread functions for each of the along and

across track directions, that is, with the notational convention of Subsection 2.4, for any $z \in \mathbb{R}$,

$$h2(v)(z) = \int_{\mathbb{R}} h1(v)(u)\mathfrak{h}_v(z-u)du. \quad (32)$$

In other words, $h2(v)$ is the result of the convolution product of $h1(v)$ and \mathfrak{h}_v .

Let us assume that, in both directions and for both sensors, the 1-D adaptive point spread function, say h , is “centered” at v ($v = (0, 0)$), with respect to the coordinate system used in Expression (6)), that is, satisfies, for any $v \in S$,

$$\left(\int_{\mathbb{R}} uh(v)(u)du \right) / \left(\int_{\mathbb{R}} h(v)(u)du \right) = 0. \quad (33)$$

In this case, in both directions, the solution \mathfrak{h}_v satisfies, for any $v \in \mathbb{R}$,

$$\left(\int_{\mathbb{R}} z\mathfrak{h}_v(z)dz \right) / \left(\int_{\mathbb{R}} \mathfrak{h}_v(z)dz \right) = 0. \quad (34)$$

Let σ_1^2 , σ_2^2 and σ^2 be the real valued functions defined on S and such that their values at v in S are the variances of the functions $h1(v)$, $h2(v)$ and \mathfrak{h}_v , respectively.

We have, for any $v \in S$,

$$\sigma_2^2(v) = \left(\int_{\mathbb{R}} z^2 h2(v)(z)dz \right) / \left(\int_{\mathbb{R}} h2(v)(z)dz \right) \quad (35)$$

(from Expressions (7), (8) and (33))

$$= \left(\int_{\mathbb{R}} z^2 \int_{\mathbb{R}} h1(v)(u)\mathfrak{h}_v(z-u)dudz \right) / \left(\int_{\mathbb{R}} h2(v)(z)dz \right) \quad (36)$$

(from Expression (32))

$$= \left(\int_{\mathbb{R}} h1(v)(u) \int_{\mathbb{R}} z^2 \mathfrak{h}_v(z-u) dz du \right) / \left(\int_{\mathbb{R}} h1(v)(u) du \right) \left(\int_{\mathbb{R}} \mathfrak{h}_v(z) dz \right) \quad (37)$$

(by the distributivity property and a convolution property)

$$= \left(\int_{\mathbb{R}} h1(v)(u) (\mathfrak{O}^2(v) + u^2) du \right) / \left(\int_{\mathbb{R}} h1(v)(u) du \right) \quad (38)$$

(from Expressions (7), (8) and (34))

$$= \left(\int_{\mathbb{R}} h1(v)(u) \mathfrak{O}^2(v) du + \int_{\mathbb{R}} u^2 h1(v)(u) du \right) / \left(\int_{\mathbb{R}} h1(v)(u) du \right) \quad (39)$$

$$= \mathfrak{O}^2(v) + \sigma 1^2(v) \quad (\text{from Expressions (7), (8) and (33)}) \quad (40)$$

Therefore, from Expressions (35) to (40), we have the following variances property, for any $v \in S$,

$$\sigma 2^2(v) = \mathfrak{O}^2(v) + \sigma 1^2(v). \quad (41)$$

Expression (41) is actually the Bienaymé equality (Loève, 1955, p.12) of the Probability Theory. From Expression (41), we see that a *necessary* condition to guarantee the existence of the solution \mathfrak{h}_v in equation (31) is

$$\sigma 1^2(v) \leq \sigma 2^2(v). \quad (42)$$

Furthermore, when $h1(v)$ and $h2(v)$ are two *Gaussian* functions, we know (e.g., by using the convolution theorem of the Fourier Transform Theory (Jain, 1989)) that the solution \mathfrak{h}_v is also a *Gaussian* function.

3.2 – CONTINUOUS SIMULATION PROCESS

Let Sensor1 and Sensor2 be the two sensors of Subsection 3.1. We are now considering the simulation of Sensor2 through the composition of a linear filter with Sensor1.

By assuming that the adaptive point spread function h_1 for Sensor1 is the same for all the images, that is, it does not depend on i , and by using the result illustrated on Figure 13, we can derive the continuous simulation process for Sensor2 shown in Figure 14.

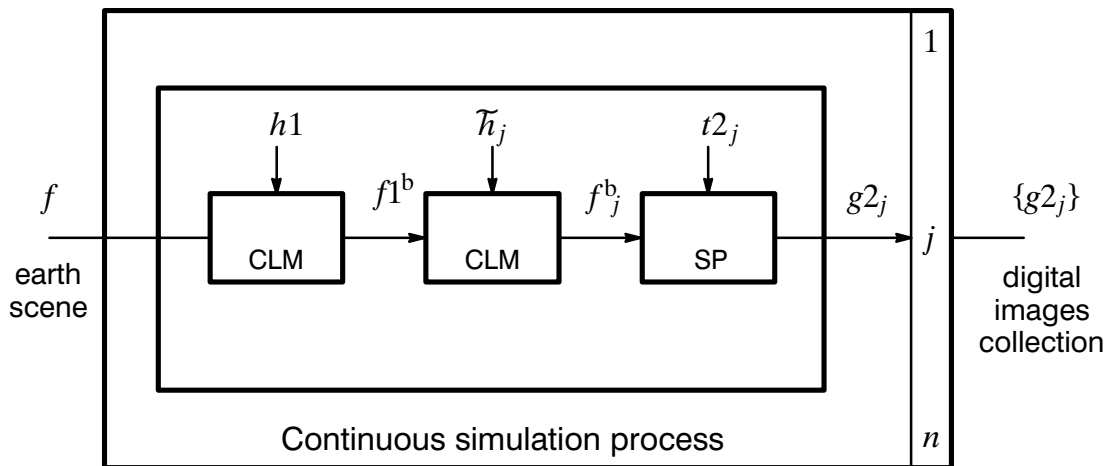
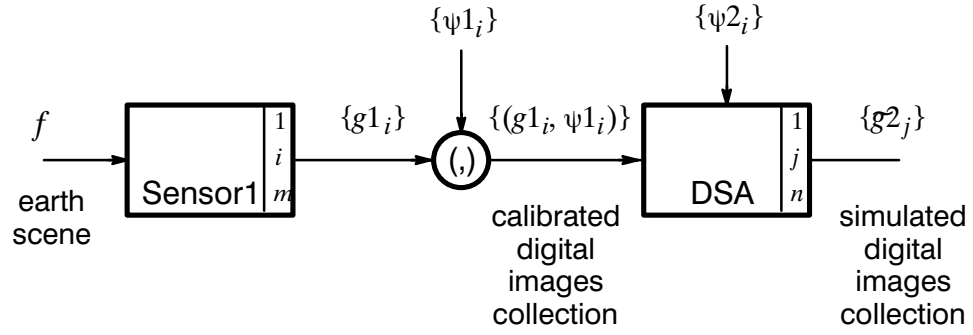


Fig. 14. Continuous simulation process for Sensor2.

The continuous simulation process is based on the blurred earth scene f_1^b relative to Sensor1 and cannot be implemented unless f_1^b is reconstructed from its samples. In the next subsection we propose a digital simulation process that avoids the explicit reconstruction of f_1^b .

3.3 – DIGITAL SIMULATION PROCESS

In place of the continuous simulation process, we propose the digital simulation process shown in Figure 15. Instead of the digital images collection $\{g_{2_j}\}$, the



DSA: Digital Simulation Algorithm

Fig. 15. Digital simulation process for Sensor2.

digital simulation process produces a simulated digital images collection denoted $\{g_{2_j}\}$, that should be a good approximation of $\{g_{2_j}\}$.

The simulated digital images collection is the result of the transformation of a collection of calibrated digital images produced by Sensor1 through a *Digital Simulation Algorithm* (DSA) which design depends on Sensor2 model.

We will denote a collection of m calibrated digital images produced by Sensor1 by $\{(g_{1_i}, \psi_{1_i})\}_1^m$ and a collection of n simulated digital images produced by the DSA by $\{g_{2_j}\}_1^n$.

A *calibrated digital image* (g_1, ψ_1) is a pair formed by a digital image g_1 , produced by Sensor1 observing an earth scene f , and the function ψ_1 given by Expression (1) that transforms f into g_1 . In other words, for each calibrated digital image (g_1, ψ_1) , together with g_1 , we know the geometrical function t_1 and the adaptive point spread function h_1 that participate in the definition of ψ_1 . In the digital simulation process, the calibrated digital images collection $\{(g_{1_i}, \psi_{1_i})\}$ is used by the DSA in place of the blurred image f_1^b

Let us denote by $E1$ and $E2$ the domains of the images produced by Sensor1 and Sensor2, respectively. The DSA for Sensor2 is then given by, for any calibrated digital images collection $\{(g1_i, \psi1_i)\}_1^m$, any $y \in E2$ and any $j = 1, \dots, n$,

$$\mathfrak{g}2_j(y) = \begin{cases} \frac{\sum_{i \in I_j(y)} \sum_{v \in E1} g1_i(v) h_{i,j}(v)(y)}{\sum_{i \in I_j(y)} \sum_{v \in E1} h_{i,j}(v)(y)} & \text{if } I_j(y) \neq \emptyset \\ 0 & \text{otherwise,} \end{cases} \quad (43)$$

where $I_j(y)$ are the sets of indices given by

$$I_j(y) = \{i \in \{1, \dots, m\} : t2_j(y) \in B_i\}, \quad (44)$$

where

$$B_i = t1_i(\text{bounding rectangle in } \mathbb{R}^2 \text{ that contains } E1); \quad (45)$$

where $h_{i,j}$ are functions from $E2$ to \mathbb{R}^{E1} .

In other words, for any pixel position y in $E2$, the digital simulation algorithm produces the pixel value $\mathfrak{g}2_j(y)$ of the simulated digital image from (if any) the calibrated digital images $(g1_i, \psi1_i)$ that cover $t2(y)$ in the sense that $t2(y) \in B_i$. Figure 16 shows a pair i, j in such situation.

In Expression (43), the functions $h_{i,j}$ can be seen as adaptive discrete point spread functions of batteries of adaptive discrete linear filters that transform the digital images $g1_i$ in \mathbb{R}^{E1} into a digital image $\mathfrak{g}2_j$ in \mathbb{R}^{E2} . For a given $y \in E2$, any $j = 1, \dots, n$ and any $i \in I_j(y)$, such functions are given by

$$h_{i,j}(v)(y) = h_y(y_{i,j} - v) \quad (v \in E1), \quad (46)$$

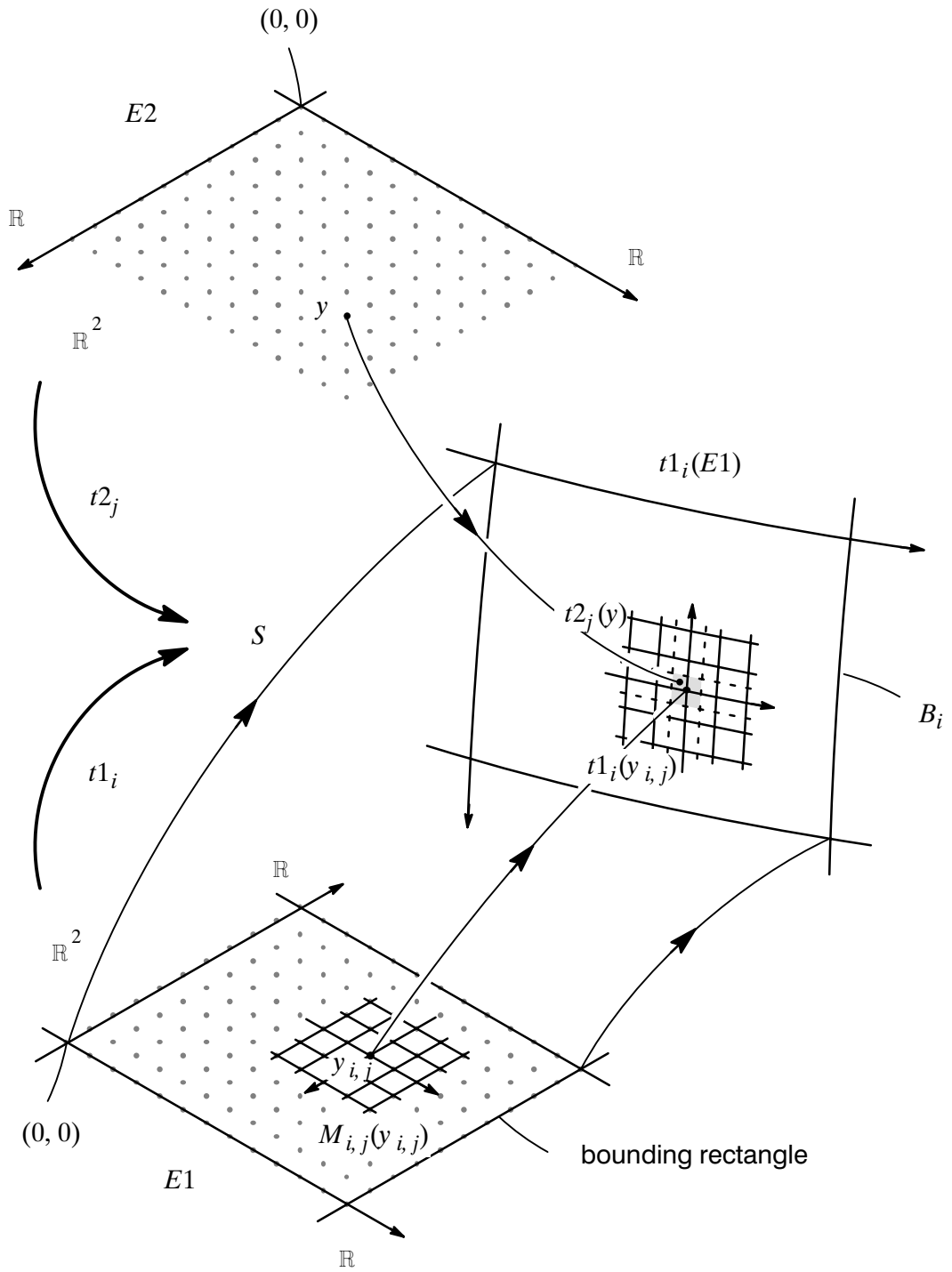


Fig. 16. Geometrical data involved in the digital simulation algorithm.

where $y_{i,j}$ are elements of E_1 such that $t1_i(y_{i,j})$ is the *nearest neighbor* of $t2_j(y)$ among $t1_i(E_1)$ (the set of all the projections of pixel positions of $g1_i$) as shown in Figure 16;

where h_y are functions from \mathbb{Z}^2 to \mathbb{R} that we call the *local point spread functions*.

Here, the use of the nearest neighbor rule is convenient because it corresponds to an implicit use of a zero order interpolator for the $f2^b$ reconstruction. Since the most significant frequencies of $f2^b$ lie below half the sampling frequency of Sensor1, this zero order interpolator would behave as an ideal interpolator and would lead to an almost perfect reconstruction of $f2^b$.

Let M be the *support* of h_y , that is,

$$M = \{z \in \mathbb{Z}^2: h_y(z) \neq 0\}. \quad (47)$$

Figure 17 shows a typical graph of h_y restricted to M .

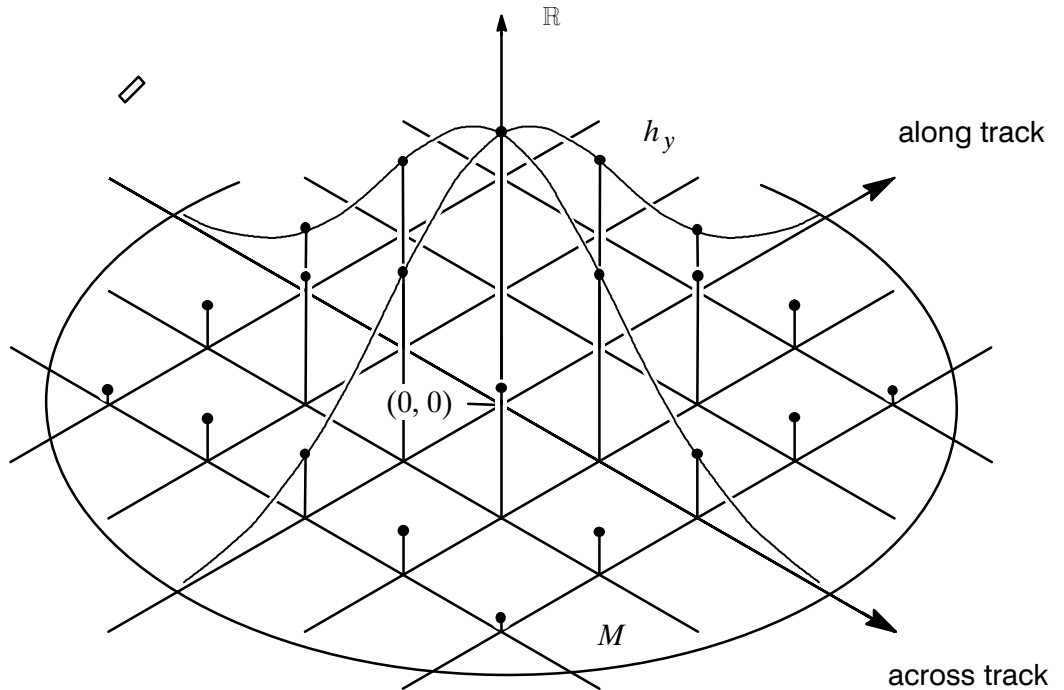


Fig. 17. Graph of h_y restricted to M (the grid nodes).

In Figure 16, we have represented the set $M_{i,j}(y_{i,j})$ defined by

$$M_{i,j}(y_{i,j}) = (M^t)_{y_{i,j}} \cap E1 \quad (48)$$

where $(M^t)_{y_{i,j}}$ represents the translate by $y_{i,j}$ of the transpose of M , that is,

$$(M^t)_{y_{i,j}} = \{y_{i,j} - z : z \in M\}. \quad (49)$$

Actually, $M_{i,j}(y_{i,j})$ is the support of $h_{i,j}(\bullet)(y)$, therefore, from Expressions (46) – (49), Expression (43) becomes

$$g2_j(y) = \begin{cases} \frac{\sum_{i \in I_j(y)} \sum_{v \in M_{i,j}(y_{i,j})} g1_i(v) h_y(y_{i,j} - v)}{\sum_{i \in I_j(y)} \sum_{v \in M_{i,j}(y_{i,j})} h_y(y_{i,j} - v)} & \text{if } I_j(y) \neq \emptyset \\ 0 & \text{otherwise,} \end{cases} \quad (50)$$

In the next subsection, we investigate a technique to design the adaptive discrete linear filters represented by the $h_{i,j}$, and ultimately by the local point spread function h_y .

4 DIGITAL FILTER DESIGN

Let h be a function from \mathbb{Z} to \mathbb{R} . As in the continuous case (see Subsection 2.4), the *variance of the function h* denoted by $\text{var}(h)$ is the positive real number given by

$$\text{var}(h) = \left(\sum_{k \in \mathbb{Z}} (k - \mu)^2 h(k) \right) / \left(\sum_{k \in \mathbb{Z}} h(k) \right), \quad (51)$$

where

$$\mu = \left(\sum_{k \in \mathbb{Z}} kh(k) \right) / \left(\sum_{k \in \mathbb{Z}} h(k) \right). \quad (52)$$

We denote by $sd(h)$ the *standard deviation* of h , that is the square root of $var(h)$.

In order to simulate properly the large-field-of-view Sensor2 from the smaller field of view Sensor1, we will use the previous assumptions made on passive sensor model and we will consider some other ones.

We will assume that Sensor1 field of view is sufficiently small compared to the earth surface in order to admit that, around a point y in $E1$, the geometrical transformation $t1$ is a *linear* transformation from \mathbb{R}^2 to the tangent plane in $t1(y)$ at the earth surface S , that is, for any $\alpha \in \mathbb{R}$, we have

$$t1(\alpha y) = \alpha t1(y) \quad (y \in \mathbb{R}^2). \quad (53)$$

We will assume that the distance between two consecutive sample positions is δ in both directions. With this assumption the geometrical transformations $t1_i$ are completely characterized by

$$t1((1, 1)) = (\delta, \delta). \quad (54)$$

We will assume that the local point spread functions h_y of Subsection 3.3 are separable. We will denote simply by h any of both corresponding 1-D functions from \mathbb{Z} to \mathbb{R} , as we did in Subsection 2.4. We will refer to h as a *point spread function*.

The Gaussian assumption on the 1-D functions $h1(v)$ and $h2(v)$, and ultimately \tilde{h}_v of Subsection 3.1 suggests (see Banon 1990 and Santos 1992) to write the point spread function h in the following form

$$h = h' \underset{*}{\overset{(1)}{}} \dots \underset{*}{\overset{(n-1)}}{h'}, \quad (55)$$

where $\underset{*}{\overset{(i)}}{}$ denote the i^{th} convolution product;

where n is a positive integer that indicates the *number minus one of convolution products* in Expression (55), $n = 1$ meaning no convolution product and simply $h = h'$;

with h' given by, for any $k \in \mathbb{Z}$,

$$h'(k) = \begin{cases} aw^{k^2} & \text{if } k \in K_N \\ 0 & \text{otherwise,} \end{cases} \quad (56)$$

where K_N , the support of k' , is given by

$$K_N = \{k \in \mathbb{Z} : |k| \leq (N-1)/2\} \text{ with the support size } N = 2l + 1 \text{ and } l \in \mathbb{N};$$

where $w \in (0, 1) \subset \mathbb{R}$;

where $a \in \mathbb{R}^+$ is a gain value such that

$$\sum_{k \in K_N} h'(k) = 1. \quad (57)$$

The representation of the point spread function h as a convolution product extended to n identical function h' is a valuable feature for designing h . In most image processing computational platform, the number N of coefficients that can be entered is bounded above (e.g., $N \leq 7$) and the variance specification for h can then be achieved by repeating $n - 1$ times the filtering operation characterized by h' .

The value of a that satisfies Expression (57) is given by

$$a = 1 / \sum_{k \in K_N} w^{k^2}. \quad (58)$$

From Expression (51) and Bienaymé equality, the variance of the above function h is given by

$$\text{var}(h) = \frac{2n(\sum k^2 w^{k^2})}{1 + 2(\sum w^{k^2})}, \quad (59)$$

where the sum is over the set $K_{N^+} = \{k \in K_N: k > 0\}$.

The correct *simulation condition* for $h_2(y)$ is obtained when the expression below is satisfied

$$t_1(\text{sd}(h)) = \mathfrak{T}(t_2(y)). \quad (60)$$

In other words, the standard deviation projection of h on the earth surface is equal to the standard deviation of \mathfrak{h}_v of Section 3 (with $v = t_2(y)$).

In Expression (60), $t_1(\text{sd}(h))$ should be written $t_1((\text{sd}(h), 0))$ or $t_1((0, \text{sd}(h)))$ depending on the chosen direction.

From Expressions (53) and (54), an equivalent simulation condition can be obtained from

$$\frac{\sigma^2}{\delta^2} = \frac{2n(\sum k^2 w^{k^2})}{1 + 2(\sum w^{k^2})}, \quad (61)$$

where σ stands for $\mathfrak{T}(t_2(y))$.

Given σ, δ, N and n , we are interested in finding the parameter w that satisfies Expression (61). We observe that Expression (61) can be written as a polynomial equation in w (of degree $((N-1)/2)^2$),

$$(\sigma^2/2) + \sum_{k \in K_{N^+}} (\sigma^2 - n\delta^2 k^2) w^{k^2} = 0. \quad (62)$$

Solving Equation (62) in w with the restriction that $w \in (0, 1)$ leads to the determination of h (and therefore of h_y and $h_{i,j}$) through the Expressions (55), (56) and (58). For $N=3$ the above equation is of degree one and corresponds exactly to the simulation condition presented in Banon (1990). In this case, the solution of Equation (62) is given by

$$w = \frac{\sigma^2/\delta^2}{2(n - \sigma^2/\delta^2)} \quad (63)$$

and the non zero values of function h' are

$$h'(0) = 1/(1 + 2w) \text{ and } h'(-1) = h'(1) = w/(1 + 2w). \quad (64)$$

Let f be the polynomial function defined by

$$f(w) = c_0 + \sum_{k \in K_{N+}} c_k w^{k^2} \quad (65)$$

with

$$c_0 = -\sigma^2/2, \quad (66)$$

and

$$c_k = n\delta^2 k^2 - \sigma^2. \quad (67)$$

An equivalent simulation condition is then given by the polynomial equation

$$f(w) = 0. \quad (68)$$

The polynomial equation (68) has $(N - 1)/2)^2$ roots. The Descartes Rule (Marins, 1985) says that the number of real positive roots of a polynomial equation, with real coefficients, is never greater than the number of signal changes in the sequence of its non zero coefficients, and if it is less, then it is even. Therefore, the equation $f(w) = 0$ has *no more than one* real positive root, since by Expressions (66) and (67) c_0 is negative and $c_1, \dots, c_{(N-1)/2}$ is an increasing sequence of real numbers, indicating that if there exists one signal change, then it is unique.

The polynomial function f is continuous in the $(0, 1)$ interval and $f(0) = c_0 < 0$, then, by Bolzano Theorem (Cláudio e Marins, 1988), a sufficient condition to have *at least one* root in this interval is

$$f(1) > 0. \quad (69)$$

Therefore, under the above condition, by Descartes Rule and Bolzano Theorem, we guarantee the existence of one and only one real positive root in the $(0, 1)$ interval for the equation $f(w) = 0$.

Figure 18 shows the graph of f for $\sigma = 96.24$, $\delta = 30$, $N = 13$ and $n = 1$.

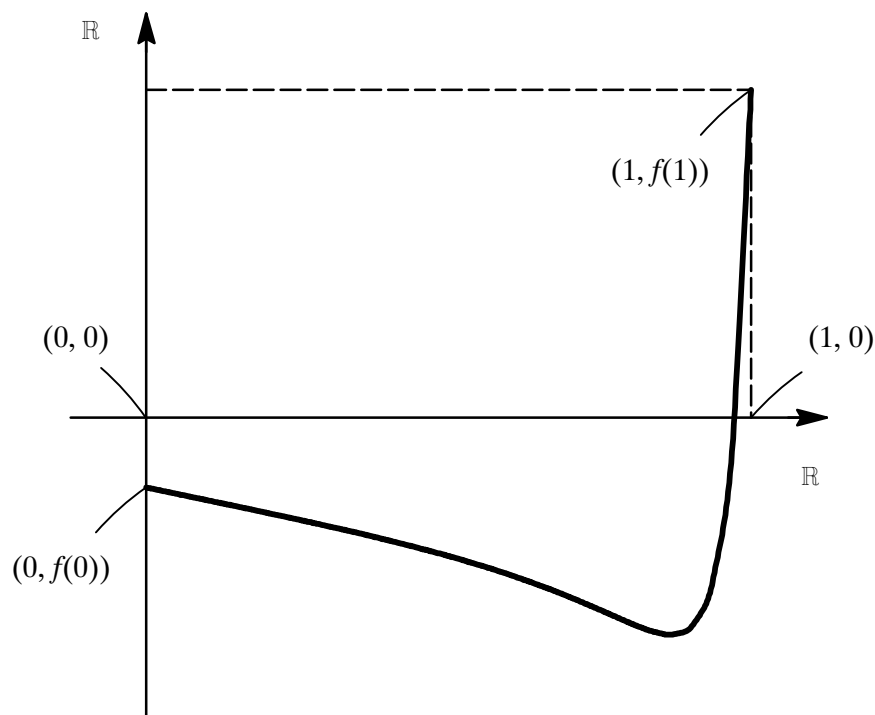


Fig. 18. Graph of f .

To solve Equation (68), we can use the Newton–Raphson method (McCracken and Dorn, 1964; Cláudio e Marins, 1988)

$$w_{i+1} = w_i - (f(w_i)/f'(w_i)) \quad i = 0, \dots \quad (70)$$

$$\text{Here } f'(w) = \sum_{k \in K_{N+}} k^2 c_k w^{(k^2-1)}.$$

Figure 18 indicates that choosing $w_0 = 1$ we should get a good precision in a few iterations.

Returning to the condition expressed in (69), we see that σ , δ , N and n must satisfy

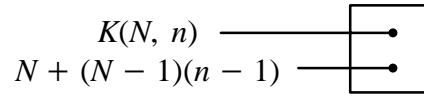
$$\frac{\sigma}{\delta} < K(N, n), \tag{71}$$

where

$$K(N, n) = ((2n/N) \left(\sum_{k \in K_{N+}} k^2 \right))^{1/2}. \tag{72}$$

Table 2 gives some typical values for $K(N, n)$ and $N + (N - 1)(n - 1)$ which represents the size, in the chosen direction, of the support M .

In order to find the filter design parameters N and n from the parameter σ and δ , we just have to read in Table 2 the values of N and n such that $K(N, n)$ is greater than σ/δ and among the possible solutions we choose the more convenient ones.

TABLE 2 – FILTER DESIGN PARAMETERS.

N	n									
	1	2	3	4	5	6	7	8	9	10
3	0.82 3	1.15 5	1.41 7	1.63 9	1.83 11	2.00 13	2.16 15	2.31 17	2.45 19	2.58 21
5	1.41 5	2.00 9	2.45 13	2.83 17	3.16 21	3.46 25	3.74 29	4.00 33	4.24 37	4.47 41
7	2.00 7	2.83 13	3.46 19	4.00 25	4.47 31	4.90 37	5.29 43	5.66 49	6.00 55	6.32 61
9	2.58 9	3.65 17	4.47 25	5.16 33	5.77 41	6.32 49	6.83 57	7.30 65	7.75 73	8.16 81
11	3.16 11	4.47 21	5.48 31	6.32 41	7.07 51	7.75 61	8.37 71	8.94 81	9.49 91	10.00 101
13	3.74 13	5.29 25	6.48 37	7.48 49	8.37 61	9.17 73	9.90 85	10.58 97	11.22 109	11.83 121
15	4.32 15	6.11 29	7.48 43	8.64 57	9.66 71	10.58 85	11.44 99	12.22 113	12.96 127	13.66 141
17	4.90 17	6.93 33	8.49 49	9.80 65	10.95 81	12.00 97	12.96 113	13.86 129	14.70 145	15.49 161

(continued).

TABLE 2

(conclusion).

N	n									
	11	12	13	14	15	16	17	18	19	20
3	2.71	2.83	2.94	3.06	3.16	3.27	3.37	3.46	3.56	3.65
	23	25	27	29	31	33	35	37	39	41
5	4.69	4.90	5.10	5.29	5.48	5.66	5.83	6.00	6.16	6.32
	45	49	53	57	61	65	69	73	77	81
7	6.63	6.93	7.21	7.48	7.70	8.00	8.25	8.49	8.72	8.94
	67	73	79	85	91	97	103	109	115	121
9	8.56	8.94	9.31	9.66	10.00	10.33	10.65	10.95	11.25	11.55
	89	97	105	113	121	129	137	145	153	161
11	10.49	10.95	11.40	11.83	12.25	12.65	13.04	13.42	13.78	14.14
	111	121	131	141	151	161	171	181	191	201
13	12.41	12.96	13.49	14.00	14.49	14.97	15.43	15.87	16.31	16.73
	133	145	157	169	181	193	205	217	229	241
15	14.33	14.97	15.58	16.17	16.73	17.28	17.81	18.33	18.83	19.32
	155	169	183	197	211	225	239	253	267	281
17	16.25	16.97	17.66	18.33	18.97	19.60	20.20	20.78	21.35	21.91
	177	193	209	225	241	257	273	289	305	321

For example, in order to find the filter design parameters N and n for $\sigma = 96.24$ and $\delta = 30$, that is, for $\sigma/\delta = 3.20$, we may choose among the following solutions (which are the best ones in terms of computer time in each line *and* column of Table 2):

$N = 3$ and $n = 16$ ($K(N, n) = 3.27$, $N^2n = 144$, $N + (N - 1)(n - 1) = 33$) or

$N = 5$ and $n = 6$ ($K(N, n) = 3.46$, $N^2n = 150$, $N + (N - 1)(n - 1) = 25$) or

$N = 7$ and $n = 3$ ($K(N, n) = 3.46$, $N^2n = 147$, $N + (N - 1)(n - 1) = 19$) or

$N = 9$ and $n = 2$ ($K(N, n) = 3.65$, $N^2n = 162$, $N + (N - 1)(n - 1) = 17$) or

$N = 7$ and $n = 3$ ($K(N, n) = 3.74$, $N^2n = 169$, $N + (N - 1)(n - 1) = 13$).

Implementation and performance considerations may orient the final choice between these five solutions.

Hence, to compute the pixel value $g_2(y)$ at position y we have to go through the following steps:

1) determination of the projection $t_2(y)$ of the pixel position y on earth (this projection can be obtained from a geometrical model for the earth, the satellite orbit, the satellite movement equation, the camera orientation and the detectors array geometrical characteristics (Santos, 1992));

2) determination of the set $I_j(y)$, that is the set of calibrated digital images (g_1, ψ_1) from Sensor1 that cover the point $t_2(y)$;

3) for such images, determination of the pixel position $y_{i,j}$ in E_1 such that $t_1(y_{i,j})$ is the nearest neighbor of $t_2(y)$ among the set of all the projections of pixel positions of g_1 ;

4) determination of $IFOV_1$ and $IFOV_2$ from Expressions (22) and (23);

5) determination of σ_1 and σ_2 from Expressions (27) and (28);

6) determination of σ for both directions, say σ_1 and σ_2 , from Expression (41), that is,

$$\sigma_1^2 = \sigma_{2_1}^2 - \sigma_{1_1}^2 \quad \text{and} \quad \sigma_2^2 = \sigma_{2_2}^2 - \sigma_{1_2}^2;$$

7) determination of N and n such that $(\max(\sigma_1, \sigma_2)/\delta) < K(N, n)$ by using, for example, Table 2;

8) determination of w from the Newton–Raphson method (70);

9) determination of h from Expressions (55), (56) and (58) for both directions, say h_1 and h_2 ;

10) determination of h_y by

$$h_y(k_1, k_2) = h_1(k_1)h_2(k_2) \quad (k_1, k_2) \in K_N^2;$$

11) determination of $\mathcal{F}_2(y)$ from Expressions (43) and (46), or (50).

In order to illustrate the above design technique, let us consider a more simple example. Let the distance between two consecutive sample positions be $\delta = 1$ and the standard deviation be $\sigma_1 = 0.46124$ for Sensor1 (i.e., $\gamma = 0.35$ for Sensor1, see Table 1). Let us assume that Sensor2 to be simulated has a resolution twice lower than Sensor1 resolution, that is $\sigma_2 = 0.92248$. From Expression (41), the standard deviation σ of the digital filter is $\sigma = \sigma_1 \sqrt{3} = 0.79889$ and, finally, $\sigma/\delta = 0.79889$. From Table 2, $N = 3$ and $n = 1$ satisfy Expression (71). In this simple case, in both directions, from Expressions (63) and (64), the non zero values of h' , that is, of h are, using matrix notation,

$$h = [0.3191 \ (0.3618) \ 0.3191], \quad (73)$$

where the element inside parenthesis corresponds to the value of h at the origin.

Figure 19 shows the graphs of the following three functions $H1$, $H2$ and $\tilde{H}2$:

$$H1(y) = \exp(-2\pi^2\sigma_1^2 y^2) \quad (y \in \mathbb{R}), \quad (74)$$

with $\sigma_1 = 0.46124$;

$$H2(y) = \exp(-2\pi^2\sigma_2^2 y^2) \quad (y \in \mathbb{R}), \quad (75)$$

with $\sigma_2 = 0.92248$;

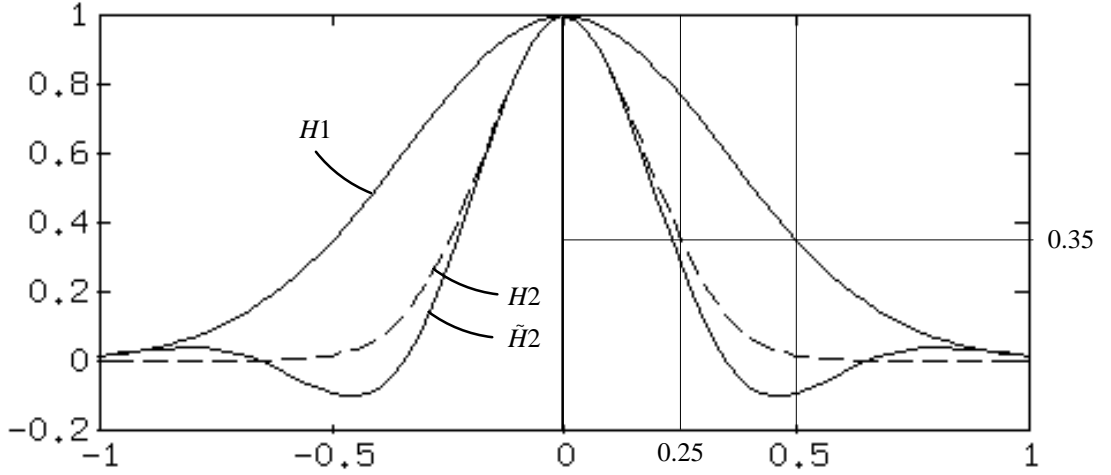


Fig. 19. Sensor1, Sensor2 and simulated Sensor2 MTF.

$$\tilde{H}2(y) = H1(y) \sum_{k \in K_3} h(k) \cos(2\pi ky) \quad (y \in \mathbb{R}), \quad (76)$$

with h given by Expression (73).

The functions $H1$, $H2$ and $\tilde{H}2$ represent the MTFs of, respectively, Sensor1, Sensor2 and the simulated Sensor2 through the composition of the design filter with Sensor1. They are the Fourier Transform of the respective point spread functions.

Finally, the 2-D digital filter point spread function is given by, using matrix notation,

$$h^t h = \begin{bmatrix} 0.1018 & 0.1154 & 0.1018 \\ 0.1154 & (0.1309) & 0.1154 \\ 0.1018 & 0.1154 & 0.1018 \end{bmatrix}.$$

5 APPLICATION TO THE BRAZILIAN REMOTE SENSING SATELLITE

The digital simulation process of Subsection 3.3 has been implemented to simulate the Remote Sensing Satellite (SSR) of the Brazilian Complete Spatial Mission (MECB) from a LANDSAT Thematic Mapper (TM) scene. In this way, band 1 and band 2 small patches have been produced.

5.1 – SSR SPECIFICATIONS

The SSR specifications that have been used (most of them can be found in Santana et al., 1988, 1989) are shown in Table 3.

TABLE 3 – SSR SPECIFICATIONS.

Parameter	Value
altitude	639.73 km
orbit inclination	82.00°
IFOV (scene element approximate size at nadir)	3.314×10^{-4} rad (212 × 212 m ²)
distance between two consecutive samples (δ) (approximate distance at nadir)	3.314×10^{-4} rad (212 × 212 m ²)
attenuation factor (γ)	0.35
number of detectors per line	3456
number of lines	3456

5.2 – SSR PATCHES SPECIFICATIONS

The SSR patches specifications that have been used are shown in Table 4. These specifications correspond to an off nadir simulation condition, as shown in Figure 20. Actually, with these specifications, the SSR patches fall entirely inside the B quadrant of the TM5 17662 image (orbit 222, point 75) of June 27, 1987.

TABLE 4 – SSR PATCHES SPECIFICATIONS.

Parameter	Value
SSR scene center latitude	- 24.69°
SSR scene center longitude	-47.88°
patch first line	SSR scene line 1
patch first column	SSR scene column 31
patch number of lines (patch projection approximate vertical dimension)	420 (89.0 km)
patch number of columns (patch projection approximate horizontal dimension)	400 (84.8 km)

The spectral characteristics of bands 1 and 2 of the SSR are assumed to be, respectively, those of bands 3 and 4 of the TM sensor.

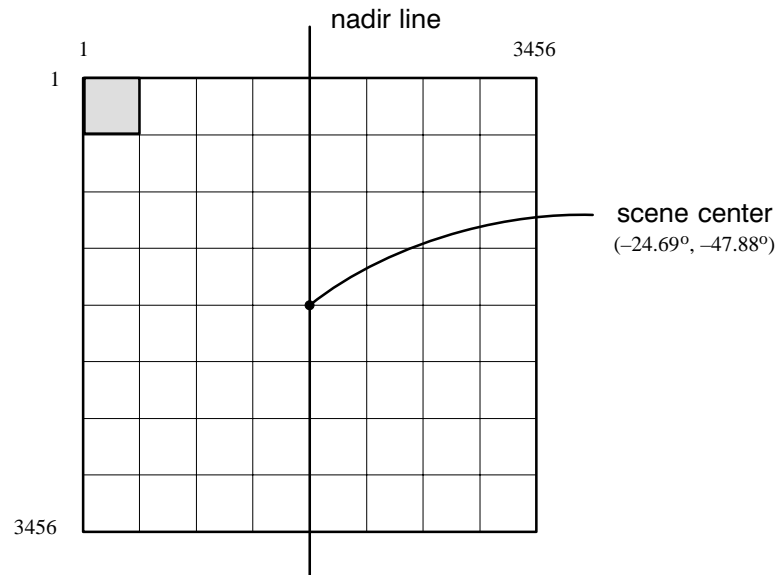


Fig. 20. Patch localization in the scene (hatch area).

5.3 – TM RESOLUTION SPECIFICATIONS

The TM resolution specifications that have been used are shown in Table 5. The EIFOV specifications can be found in Fonseca, 1988, p. 43, and Fonseca et al., 1993. The values of σ_1 are obtained from the EIFOV values through Expression (15) or Table 1.

TABLE 5 – TM RESOLUTION SPECIFICATIONS.

	Row	Column
δ	30 m	30 m
EIFOV	41.6 m	45.4 m
σ_1 (actually used) (σ_1 obtained from EIFOV)	17 m (15.59 m)	17 m (17.02 m)

5.4 – SIMULATION FILTER SPECIFICATIONS AND PERFORMANCES

The filter design parameters n and N that have been used are $n = 1$ and $N = 15$. The value $n = 1$ has been chosen because it corresponds to the most efficient solution in terms of computer time and in our implementation we did not have any upper bound for the possible values of N . The value $N = 15$ has been obtained from the evaluation of σ/δ and consulting Table 2. To compute σ/δ , we go through the following steps with respect to the point u (see Figure 12) that corresponds to the upper left corner pixel position of the SSR scene defined in Table 4:

1) the curvature radius r_c is 6381.35 km and a view angle $\theta = \text{IFOV} \times (\text{number of detectors}) / 2$ is 0.57266 rad (with $\text{IFOV} = 3.314 \times 10^{-4}$ rad and number of detectors = 3456);

2) the length of up r is 777.74 km (from Expression (24), with $h = 639.73$ km);

3) the angle ucq θ_c is 0.06609 rad (from Expression (25));

4) the IFOV_1 is 216.62 m (from Expression (22));

5) the IFOV_2 is 226.77 m (from Expression (23));

6) the standard deviation σ_2 (i.e., $\sigma_2(u)$) is 104.59 m (from Expression (28));

7) the standard deviation σ (i.e., σ_2) is 103.20 m (from Expression (41), with $\sigma_1 = 17$ m);

8) the ratio σ/δ is 3.44 (with $\delta = 30$ m).

Actually, from Table 2 (with $n = 1$), $N = 13$ is acceptable ($K(13, 1) = 3.74$). We chose $N = 15$ to get a better MTF Gaussian approximation as we see on Figure 21.

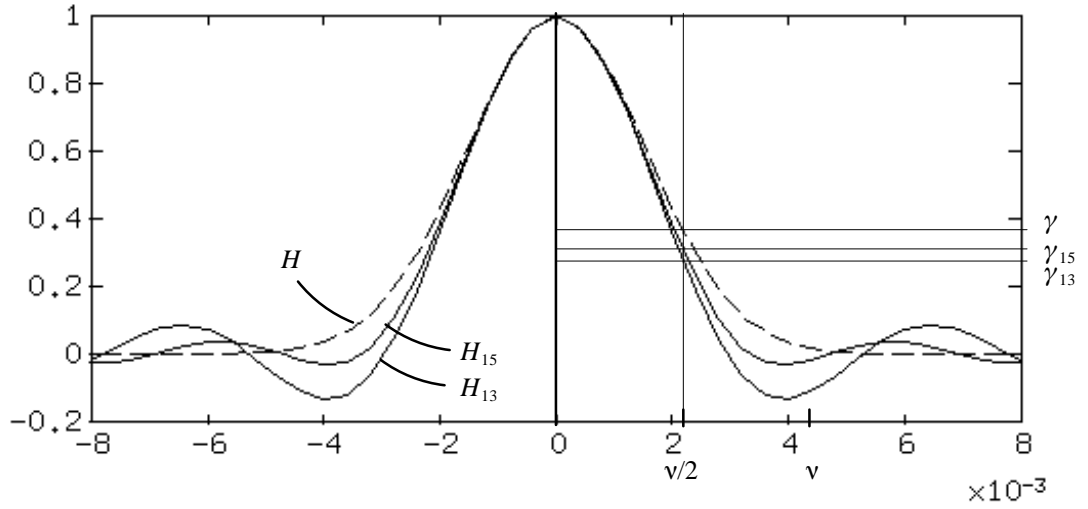


Fig. 21. MTFs' comparison.

Figure 21 shows the graphs of the following three functions H , H_{13} and H_{15} :

$$H(y) = \exp(-2\pi^2\sigma^2y^2) \quad (y \in \mathbb{R}), \quad (77)$$

with $\sigma = 103.20$;

$$H_{13}(y) = \sum_{k \in K_{13}} aw^{k^2} \cos(2\pi\delta ky) \quad (y \in \mathbb{R}), \quad (78)$$

with $w = 0.9851566098$ (from Expression (62), with $\sigma = 103.20$, $\delta = 30$, $N = 13$ and $n = 1$), $a = 0.09328127732$ (from Expression (58), with $N = 13$) and $\delta = 30$;

$$H_{15}(y) = \sum_{k \in K_{15}} aw^{k^2} \cos(2\pi\delta ky) \quad (y \in \mathbb{R}), \quad (79)$$

with $w = 0.9704356817$ (from Expression (62) with $\sigma = 103.20$, $\delta = 30$, $N = 15$ and $n = 1$), $a = 0.10458408803$ (from Expression (58), with $N = 15$) and $\delta = 30$.

The functions H , H_{13} and H_{15} represent the MTFs of, respectively, the ideal continuous filter and the digital filters with two different support sizes. They are the Fourier Transform of the respective point spread functions.

For both solutions, $N = 13$ and $N = 15$, the variances of the digital filter point spread functions h are the same by construction ($\text{var}(h) = 103.20^2$), but with a larger impulse response support, we reduce the effects of the Gibbs phenomenon resulting from truncation. With $N = 15$ instead of $N = 13$, we better fill the original specification of the continuous filter, that is, the value 0.3599 of the attenuation factor γ at half the sampling frequency $\nu = 1/226.77 = 0.0044 \text{ m}^{-1}$. From Expressions (78) and (79) (with $y = \nu/2$) we have $\gamma_{13} = 0.2692$ and $\gamma_{15} = 0.3029$.

From Figure 21, we see that the proposed digital filter behaves properly for low frequency signals and is conservative for frequencies around half the sampling frequency ($\nu/2$). In other words, the image obtained from sensor simulation will be theoretically slightly more blurred than it should be, nevertheless without practically any visual difference. Furthermore, the value $\sigma = 103.20$ corresponds to the upper left pixel simulation, for the other pixels the value of σ is smaller and the discrepancy between γ and γ_{15} decreases monotonically.

Figures 22 and 23 show, respectively, the two small patches of the band 1 and band 2 specified in Subsection 5.2 and obtained by SSR simulation from TM5 Band 3 and Band 4 (orbit 222, point 75, quadrant B, June 27, 1987). They show Buritama reservoir and Araçatuba, Birigui and Penápolis cities of São Paulo state.

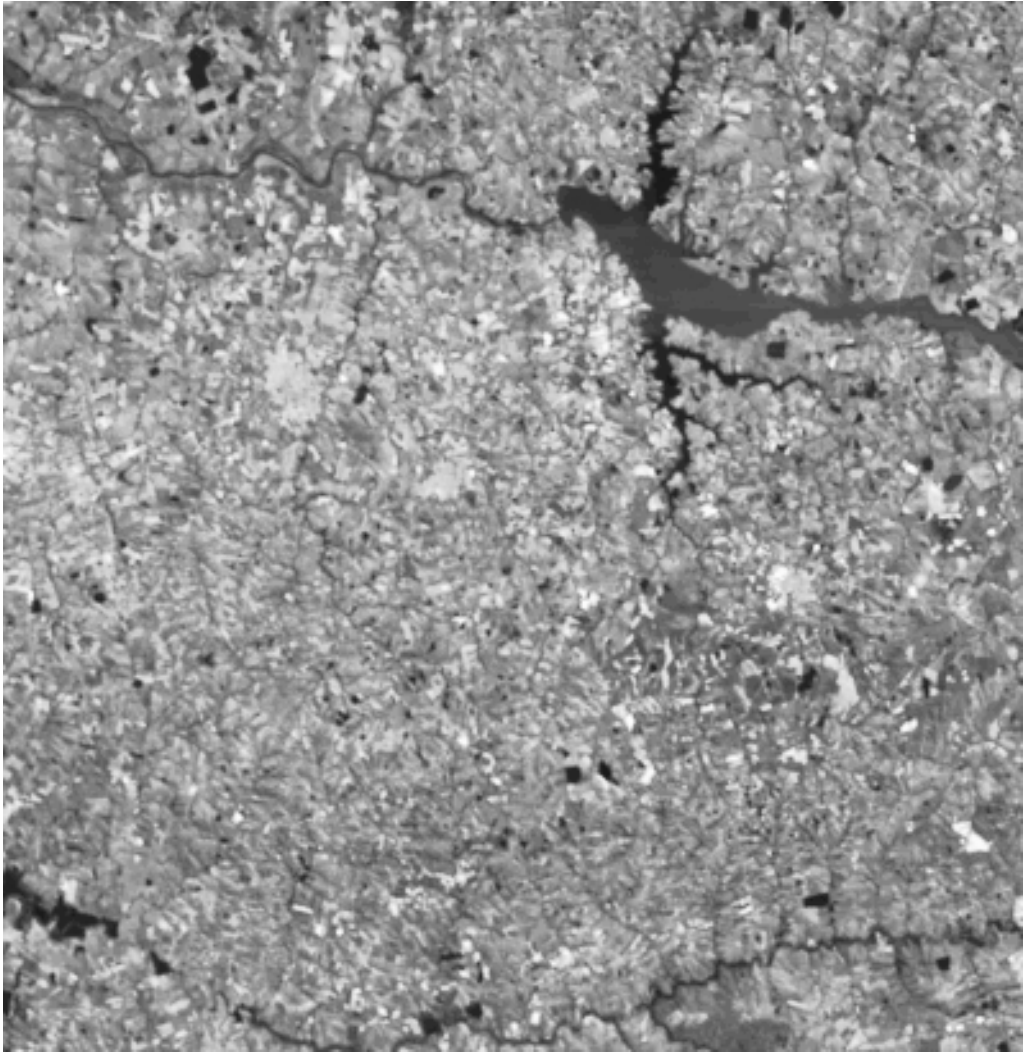


Fig. 22. Buritama reservoir and Araçatuba, Birigui e Penápolis cities (São Paulo State).
SSR Band 1 patch obtained by SSR simulation from TM5 Band 3,
orbit 222, point 75, quadrant B, June 27, 1987.

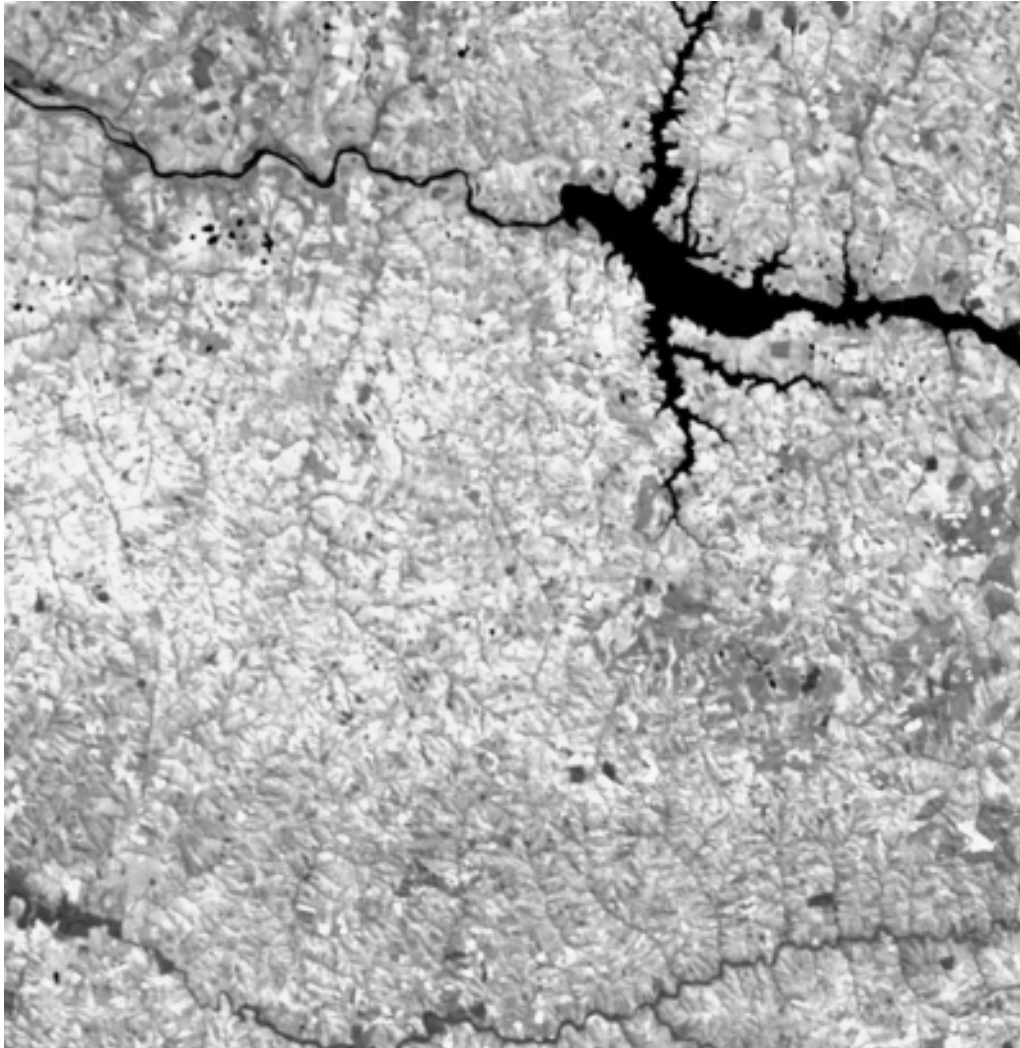


Fig. 23. Buritama reservoir and Araçatuba, Birigui e Penápolis cities (São Paulo State). SSR Band 2 patch obtained by SSR simulation from TM5 Band 4, orbit 222, point 75, quadrant B, June 27, 1987.

6 CONCLUSION

In this paper we have presented a new technique to design a linear digital filters for sensor simulation. The design technique is based on the assumption that the point spread function of the ideal continuous filter should be Gaussian and that the point spread function of the digital approximation filter should have the same variance. A numerical table has been given that is useful to determine the minimum size of the impulse response support of the filter. The study of the performance of the designed digital filter has

shown that good properties can be achieved. For any support size above the lower acceptable value the digital filter properly attenuates the low frequency components and for the frequency components around half the sampling frequency we can reach the desired precision level for the attenuation factor just by increasing the support size.

Finally, bands 1 and 2 patches of the Remote Sensing Satellite (SSR) of the Brazilian Complete Spatial Mission (MECB) have been obtained from a LANDSAT Thematic Mapper scene. The chosen orbit for the SSR is such that the patches are in off nadir acquisition conditions.

With the digital simulation process at hands, it is now possible to evaluate the future images that would be produced by the SSR (Remote Sensing Satellite) of MECB (Brazilian Complete Spatial Mission) and to test the programs that will process the raw image in order to reconstruct the original scene along a given cartographic projection.

REFERENCES

- Banon, G.J.F. Simulação de imagens de baixa resolução. **SBA: Controle & Automação**, 2(3):180–192, 1990. (in Portuguese).
- Begni, G.; Dinguirard, M.C.; Jackson, R.D.; Slater, P.N. Absolute calibration of the SPOT–1 HRV Cameras. In: **SPIE Earth Remote Sensing Using the Landsat Thematic Mapper and SPOT Sensor Systems**, Bellingham, WA, 1986. p. 66–76. (SPIE Proceedings v. 660). Technical Conference at the Third International Symposium on Optical and Optoelectronic Applied Sciences and Engineering, Innsbruck, 14–18 Apr. 1986.
- Cláudio, D.M.; Marins, J.M. **Cálculo numérico computacional**. São Paulo, Editora Atlas, 1988.
- Fonseca, L.M.G. **Restauração e interpolação de imagens do satélite Landsat por meio de técnicas de projeto de filtros FIR**. (Master thesis) – ITA, São José do Campos, Brazil, 1988. 148p. (in Portuguese).
- Fonseca, L.M.G.; Prasad, G.S.S.D.; Mascarenhas, N.D.A. Combined interpolation – restoration of Landsat images through FIR filter design techniques. Accepted for publication in the **International Journal of Remote Sensing**, 1993.
- Jain, A.K. **Fundamentals of digital image processing**. Englewood Cliffs, NJ, Prentice Hall, 1989.
- Leger, D.; Leroy, M.; Perbos, J. SPOT MTF performance evaluation. In: **SPIE Earth Remote Sensing Using the Landsat Thematic Mapper and SPOT Sensor Systems**, Bellingham, WA, 1986. p. 93–97. (SPIE Proceedings v. 660). Technical Conference at the Third International Symposium on Optical and Optoelectronic Applied Sciences and Engineering, Innsbruck, 14–18 Apr. 1986.

- Marins, J.M. Separação das raízes reais de equações polinomiais pelo método de Sturm. **Segundo Encontro Regional de Matemática Aplicada e Computacional**. São José dos Campos, Brazil, 1985. (in Portuguese).
- McCracken, D.D.; Dorn, W.S. **Numerical methods and FORTRAN programming**. New York, John Wiley, 1964.
- Santana, C.E.; Carvalho, H.C.; Kono, J. **MECB SSR1 remote sensing satellite concept review**. São José dos Campos, INPE, 1988. (MECB-SSR1-A-REV-1000.)
- Santana, C.E.; Muzzio, J.L.R.; Kono, J.; Carvalho, H.C. **MECB SSR1 imaging instrument subsystem specification**. São José dos Campos, INPE, 1989. (MECB-SSR1-A-ETC-1014).
- Santos, A.C. dos **Simulação de imagens de sensores com largo campo de visada a partir de imagens de sensores com menor campo de visada – O caso SSR/TM**. (Master thesis) – São José do Campos, INPE, 1992. 142p. (INPE-5378-TDI/473). (in Portuguese).